Ultrasonic Attenuation in Bismuth at Low Temperatures*

DARRELL H. RENEKER† ‡
Department of Physics and Institute for the Study of Metals, University of Chicago, Chicago, Illinois
(Received February 20, 1959)

The attenuation of ultrasonic waves in bismuth has been measured at frequencies between 12 and 84 Mc/sec for various orientations. The magnetic field dependence of the attenuation at low temperatures exhibits three distinct oscillatory components and a saturation region at fields between 5 and 1600 oersteds. A simple interpretation of the salient features of the observations is presented. In particular, the effective mass parameters of the electrons have been determined from the periods of the geometric resonance and de Haas-van Alphen oscillations. A method of measuring the maximum Fermi velocity in a given direction is described, and the results of such a measurement are used to determine an independent value of the Fermi energy. Some data on the temperature and frequency dependence of the zero-field attenuation are included.

I. INTRODUCTION

THE investigation reported here of the attenuation of sound waves in bismuth was originally undertaken to establish the validity of Blount's[1] two-deformation-potential model. According to this point of view, the impossibility of simultaneously screening the deformation potentials of both holes and electrons should give rise to a substantial electronic contribution to the sound attenuation at low temperatures despite a carrier density of only 10^{-5} per atom.

Initial experiments indicated the probable existence of such an electronic component in the attenuation measured in the liquid-helium temperature range. A study of the effect of a magnetic field H_0 on the attenuation was then undertaken in an effort to unravel this component from a complicated background attenuation arising from thermal agitation, impurities, dislocations and other extraneous scattering centers. The attenuation was found to depend periodically on $1/H_0$,[2] a phenomenon previously found by Bommel[3] and by Morse *et al.*[4]

It has been suggested by Pippard[5] that the periods of these oscillations are controlled by details of the band structure only qualitatively understood in most substances. It was apparent that a study of these complicated phenomena in bismuth, whose band structure has been quantitatively studied,[6–11] would provide an excellent opportunity to relate the oscillatory behavior to the band structure. Hopefully, a better understanding of the attenuation as a function of field would establish it as a useful tool in the investigation of the band structure of other materials. Accordingly, the emphasis of the experiment was shifted to a study of the magnetic-field-dependent part of the attenuation as a function of various experimental parameters.

It should be noted that most of the experimental work was carried out before an adequate theoretical model for the field dependence was available. During the course of the investigation, however, considerable theoretical progress has been made.[12–16] In the interest of clarity, we shall, therefore, not present our results in the historical order in which they were obtained, but present first, in Sec. II, a simple outline of our current theoretical understanding. In Sec. III, we describe the experimental technique with particular emphasis on the production of pure, unstrained crystals with electronic mean free paths and relaxation times sufficiently long to permit the observation of oscillatory phenomena. We also discuss the reasons for shifting from the pulse echo technique used in our initial studies of the total attenuation to a more sensitive but less direct continuous-wave technique. Data are presented in Sec. IV on three characteristically different sets of oscillations and the striking nature of their anisotropic dependence on crystal orientation. Finally, in Sec. V, these data are quantitatively related to band structure parameters with the aid of theory discussed in Sec. II.

II. THEORY

Bismuth has rhombohedral symmetry. We designate the three-fold axis by z, one of the three positive two-fold axes by x, and the corresponding bisectrix by y. The Fermi surface for electrons in bismuth consist of three sets of two ellipsoids each.[7] The three sets are interrelated by 120° rotations around z. The doubling of each set arises from inversion symmetry. One of the

* Submitted in partial fulfillment of the requirements for the degree of Ph.D. at the University of Chicago.
† Now at Polychemicals Department, E. I. du Pont and Company, Wilmington, Delaware.
‡ National Science Foundation Predoctoral Fellow.
[1] E. I. Blount, Phys. Rev. **114**, 418 (1959).
[2] D. H. Reneker, Phys. Rev. Letters **1**, 440 (1958).
[3] H. E. Bommel, Phys. Rev. **100**, 758 (1955).
[4] Morse, Bohm, and Gavenda, Phys. Rev. **109**, 1394 (1958).
[5] A. B. Pippard, Phil. Mag. **2**, 1147 (1957).
[6] B. Abeles and S. Meiboom, Phys. Rev. **101**, 544 (1956).
[7] D. Shoenberg, Proc. Roy. Soc. (London) **A170**, 341 (1939).
[8] D. Shoenberg, Phil. Trans. Roy. Soc. (London) **A245**, 1 (1952).
[9] D. Shoenberg, Phil. Trans. Roy. Soc. (London) **A248**, 1 (1955).
[10] J. E. Aubrey and R. G. Chambers, J. Phys. Chem. Solids **3**, 128 (1957).
[11] A. D. Brailsford and J. K. Galt, International Conference on the Electronic Properties of Metals at Low Temperatures, Geneva, New York, 1958 (unpublished).
[12] A. B. Pippard, Phil. Mag. **46**, 1104 (1955).
[13] M. S. Steinberg, Phys. Rev. **109**, 1486 (1958).
[14] S. Rodriguez, Phys. Rev. **112**, 80 (1958).
[15] T. Kjeldaas, Jr., Bull. Am. Phys. Soc. **3**, 180 (1958).
[16] Cohen, Harrison, and Harrison (to be published).

principal axes of each ellipsoid is parallel to a two-fold axis, which restricts the positions of the centers of the ellipsoids either to the two-fold axes or the reflection planes normal to these. The particular set of two ellipsoids with this principal axis along our x axis is given by

$$\alpha_{11}p_x^2+\alpha_{22}p_y^2+\alpha_{33}p_z^2+2\alpha_{23}p_yp_z=2m_0E_e, \quad (1)$$

where $\mathbf{p}=\hbar\mathbf{k}$ and $\mathbf{k}$ is measured relative to the center of the ellipse. Further, E_e is the Fermi energy of the electrons and the α_{ij} are the components of the reciprocal mass tensor in units of $1/m_0$.

In addition to the electrons in the conduction band, there is an equal concentration of holes in the valence band. The Fermi surface of these holes consists of two ellipsoids of revolution centered on the z axis and described by

$$\beta_{11}(p_x^2+p_y^2)+\beta_{33}p_z^2=2m_0E_h, \quad (2)$$

where E_h is the Fermi energy of the holes, the β_{ij} are the components of the reciprocal mass tensor, and $\mathbf{p}=\hbar\mathbf{k}$ with $\mathbf{k}$ now measured from the center of the hole ellipsoid.

We first discuss the general dependence of the attenuation upon H_0 when H_0 is transverse to the direction of propagation. There are five regions of field for which the dependence of the attenuation α on H_0 is characteristically different. We designate these regions as (1) the magnetoresistance, (2) the cyclotron resonance, (3) the geometric resonance, (4) the saturation, and (5) the de Haas-van Alpen regions, in order of increasing field. We now discuss each of these regions in turn, describing the characteristic behavior, its physical origin, the range of field, and the criteria for observability.

In the magnetoresistance region, α changes smoothly with H_0 as the latter increases from zero just as does the low-frequency electrical resistance. The region is limited to fields such that $\omega_c<\omega$, where ω_c is the cyclotron resonance frequency discussed in more detail below and ω the circular frequency of the sound wave. For the frequencies used in our experiments on Bi, the magnetoresistance range occurred well below the smallest value of H_0 employed. In any event, the criterion for significant change of α in this region, $\omega\tau\gg1$, where τ is a typical relaxation time of the carriers, is not satisfied in these experiments. We therefore did not concern ourselves with this phenomenon.

The cyclotron resonance absorption, familiar in the case of electromagnetic waves,[17] can in principle occur also for ultrasonic waves.[18] The usual Bohr frequency condition,

$$\omega=n\omega_c, \quad (3)$$

fixes the values of H_0 for possible resonance, where

$$\omega_c=eH_0/m^*c. \quad (4)$$

In Eq. (4), m^* is an appropriate effective mass which depends in general upon the orientation of H_0. According to Eq. (3) and Eq. (4), the absorption is periodic in $1/H_0$ with a period given by

$$\Delta(1/H_0)=e/\omega m^*c, \quad (5)$$

and the fundamental value of H_0 is equal to the reciprocal of the period.

The position of the fundamental was estimated from Aubrey's[19] values of the effective masses for the electrons. For the frequencies used here, the cyclotron resonance for the electrons occurs for fields in the range 0.1 to 1 oersteds, which are lower than our experimental range. The criterion for observation, $\omega\tau\gg1$, is not satisfied. Preliminary values for the mass parameters of holes obtained in this laboratory from anomalous skin effect measurements[20] indicate that the fundamental occurs in the range 4 to 12 oersteds. Estimates of τ for the holes indicate that their cyclotron resonance might just barely be observable.

Pippard[12] has suggested that a geometric resonance (previously called magnetoacoustic resonance[2]) should occur when the diameter d of the carrier orbits is an "odd multiple of half-wavelengths" and has proposed this as an explanation of the effects first observed by Bommel.[3]

The detailed theory in the form developed by Cohen, Harrison, and Harrison[16] confirms this suggestion of Pippard but indicates the resonance condition is actually

$$d=2p_fc/eH_0\cong n\lambda, \quad (6)$$

where d is the orbital diameter of an electron at the Fermi surface and p_f the Fermi momentum. The periods in $1/H_0$ thus scale with λ rather than $1/\omega$ as is the case for cyclotron resonance. The physical origin of the attenuation lies in the dissipation through collisions of the kinetic energy associated with displacement and distortion of the orbit by the sound wave. It is the amplitude of this displacement which becomes a maximum at geometric resonance. When the displacement amplitude is a maximum, the electrons follow the motion of the lattice most effectively and the attenuation is a minimum. Thus Eq. (6) gives approximately for small n and more accurately for large n the values of H_0 for minimum attenuation. The condition expressed in Eq. (6) implies that $n\omega_c=(v_f/v_s)\omega$, where v_f is the Fermi velocity and v_s the velocity of sound. The fields at which geometric resonances occur are therefore of order v_f/v_s greater than those for cyclotron resonance and fall within the experimental range for bismuth. The condition for large amplitude of oscillation is that $\omega_c\tau\gg1$. From Eq. (6) this requirement is equivalent to $ql\gg1$. Because $ql=(v_f/v_s)\omega\tau$, the purity required for geometric resonance is far more readily

[17] Dresselhaus, Kip, and Kittel, Phys. Rev. **98**, 368 (1955).
[18] N. Mikoshiba, J. Phys. Soc. Japan **13**, 759 (1958).
[19] J. E. Aubrey (private communication).
[20] G. Smith (private communication).

attained than that required for cyclotron resonance at a given frequency.

The detailed theory has only been developed for the electron gas. For small ellipsoidal Fermi surfaces, the dynamical aspects of the theory are unchanged except for the introduction of anisotropy. The determination of the electromagnetic field associated with the sound wave and hence of α from the dynamics *is* completely altered by the presence of several ellipsoids of electrons and holes. Nevertheless, it is only the dynamical aspect which need be invoked to establish the existence of cyclotron resonance and geometric resonance.

If we now redefine d to be the maximum extension of the now ellipsoidal orbit in the direction of propagation, the condition for geometric resonance expressed by Eq. (6) can be taken over unaltered. Onsager[21] has pointed out that the orbit in coordinate space is the same as the orbit in momentum space except for a rotation of 90° about H_0 and a scale factor of c/eH. This fact enables one to obtain simply the connection between the observed periods and the extension of the Fermi surface in $\mathbf{p}$ space. We now specialize to bismuth and consider the case $\mathbf{q}$ along x, H_0 at an angle θ from the z axis in the y,z plane. The two ellipsoids described by Eq. (1) gives one set of periods, and the two remaining pairs of ellipsoids give a second set of coincident periods. The values of the momenta to be substituted for p_f in Eq. (6) are

$$p_1{}^x=\frac{2(m_0E_e)^{\frac{1}{2}}}{[(\alpha_{22}+\alpha_{33})+(\alpha_{22}-\alpha_{33})\cos 2\theta-2\alpha_{23}\sin 2\theta]^{\frac{1}{2}}}, \quad (7)$$

for the first pair of ellipsoids and

$$p_{2,3}{}^x=2[m_0E_e(\alpha_{11}+3\alpha_{22})]^{\frac{1}{2}}\times[(4\alpha_{11}\alpha_{22}+\alpha_{33}\alpha_{11}+3\alpha_{22}\alpha_{33}-3\alpha_{23}{}^2)+(4a_{11}\alpha_{22}-\alpha_{33}\alpha_{11}-3\alpha_{22}\alpha_{33}+3\alpha_{23}{}^2)\cos 2\theta+4\alpha_{23}\alpha_{11}\sin 2\theta]^{-\frac{1}{2}} \quad (8)$$

for the two remaining pairs. The corresponding expression for holes is

$$p_h{}^x=\frac{2(m_0E_h)^{\frac{1}{2}}}{[\beta_{11}+\beta_{33}+(\beta_{11}-\beta_{33})\cos 2\theta]^{\frac{1}{2}}}. \quad (9)$$

Values of p^x for the various carriers have been computed from the values of α_{ij}, β_{ij}, E_e, and E_h listed with their sources in Table VI. In particular for H_0 along y and z, the values of H_0 for geometric resonance obtained from this calculation are indicated schematically in Fig. 1(a) and (b), respectively.

The requirement that l be greater than λ is well satisfied for electrons at 60 Mc/sec but is marginal even in the best samples at 12 Mc/sec. The condition is barely satisfied for holes even at 60 Mc/sec.

As the field increases further, the orbital diameter becomes smaller than λ, $d=2p_fe/cH<\lambda$. The force exerted by the sound wave becomes independent of the position of the electron in its orbit, and no further field dependence associated with purely classical effects can occur. The existing theory is insufficient to establish the saturation value of α for bismuth. The saturation region is also indicated schematically in Fig. 1(a) and Fig. 1(b). When l is less than λ, however, saturation occurs when $d<l$.

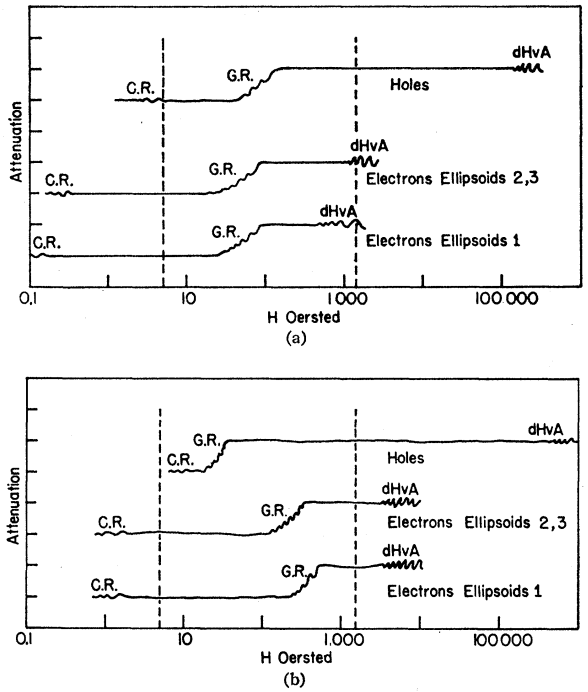

FIG. 1. (a)–(b) Predicted fields for occurrence of various oscillatory phenomena. (a) $H_0\|y$. (b) $H_0\|z$, 60 Mc/sec longitudinal mode along x. C. R. is cyclotron resonance; G. R. is geometric resonance; the step indicates saturation, and dHvA refers to de Haas-van Alphen. The oscillations are indicated only schematically. Electron ellipsoid 1 as given in Eq. (1); electron ellipsoids 2 and 3 are Eq. (1) rotated ±120° about the z axis.

Thus far all our considerations have been classical. When the energy separation between adjacent Landau levels $\hbar\omega_c$ becomes comparable to KT where K is the Boltzmann constant, this semiclassical approximation breaks down. De Haas-van Alphen oscillations set in just as in the magnetic susceptibility and a wide variety of transport properties.[22,23] One period in $1/H_0$ for the electrons of Eq. (1) for the particular case in which H_0 is in the x,y plane at an angle φ from x is given by

$$\Delta\frac{1}{H}=\frac{e\hbar}{m_0cE_e}[\alpha_{11}\alpha_{33}+(\alpha_{22}\alpha_{33}-\alpha_{11}\alpha_{33}-\alpha_{23}{}^2)\cos^2\varphi]^{\frac{1}{2}}. \quad (10)$$

Two other periods, corresponding to the choice of φ differing by ±120° in Eq. (10), simultaneously occur,

[21] L. Onsager, Phil. Mag. **43**, 1006 (1952).

[22] D. Shoenberg, *Progress in Low-Temperature Physics* (North-Holland Publishing Company, Amsterdam, 1957), Vol. II, p. 225.

[23] J. P. Jan, *Solid-State Physics*, edited by F. Seitz and D. Turnbull (Academic Press, Inc., New York, 1957), Vol. 5, p. 1.

corresponding to the fact that a plane perpendicular to H_0 can cut the three sets of ellipsoids at different angles.

The hole periods are independent of φ and are given by

$$\Delta 1/H = e\hbar(\beta_{11}\beta_{33})^{\frac{1}{2}}/m_0 c E_h. \quad (11)$$

These oscillations should in principle be observed at all fields up to a maximum field which is given by the reciprocal of the period. However, the amplitude of the oscillations is damped by a factor $\exp\{-(2\pi Kc/eh) \times (Tm^*/H)\}$ and consequently the oscillations are only observed at very low temperatures and at the values of H_0 near $[\Delta(1/H_0)]^{-1}$.

Using preliminary data for one situation, this exponential factor may be used to estimate the minimum fields at which these oscillations might be observed under a variety of conditions, and these values are shown schematically in Fig. 1(a) and Fig. 1(b). For $H_0=1600$ oersteds, the maximum field employed in this work, the oscillations due to the electrons should be observable for all field directions except those within a cone around the z axis of half angle 45°. The period and amplitude considerations indicate that the oscillations associated with the holes would only be visible for $H_0>10^5$ oersteds.

Thus far we have supposed $\mathbf{H}_0\cdot\mathbf{q}=0$ so that there is a slow advance of planes of constant phase past the electrons spiralling along H_0. When the field is tipped towards the direction of propagation, the average drift velocity of a carrier along $\mathbf{H}_0$, $\mathbf{v}_H$ has a component along $\mathbf{q}$. The phase velocity relative to the carrier is reduced from v_s to $v_s-v_H\sin\nu$, where $\pi/2-\nu$ is the angle between $\mathbf{q}$ and $\mathbf{H}_0$. If the condition

$$v_s = v_H \sin\nu \quad (12)$$

is satisfied, the carrier experiences a steady acceleration because the orbital average of the force exerted on the carrier remains constant in phase. The contribution to the attenuation of the carriers for which (12) is satisfied can therefore become very large. Consider now the saturation region where $d\ll\lambda$. As ν increases from zero, $v_H\sin\nu$ is initially smaller than v_s even for carriers having the maximum v_H. At a certain critical angle ν_c,

$$\sin\nu_c = v_s/v_{H\,\max}, \quad (13)$$

the carriers at the Fermi surface having the maximum v_H can just satisfy (12). The attenuation should then increase as ν increases beyond ν_c. Because collisions destroy the phase relation between carrier and sound wave, $\omega\tau\gg1$ is the criterion for an abrupt increase in α with ν setting in at $\nu=\nu_c$. For electrons in bismuth with $\mathbf{q}$ along x, $\mathbf{H}_0$ in the x-y plane, and ν the angle between $\mathbf{H}_0$ and y, the dependence of $(v_H)_{\max}$ on ν is

$$(v_H)_{\max}\cong\left[\frac{2\alpha_{33}E_e}{m_0(\alpha_{22}\alpha_{33}-\alpha_{23}^2)}\right]^{\frac{1}{2}}(\alpha_{11}\sin^2\nu+\alpha_{22}\cos^2\nu), \quad (14)$$

for the set of ellipsoids [Eq. (1)] having smallest $(v_H)_{\max}$. The maximum velocity of sound in bismuth is 2.6×10^5 cm/sec for longitudinal waves along x. For this value of v_s, a value of $E_e=0.017_7$ ev, and Aubrey's values for α_{ij}, Eqs. (13) and (14) yield 1° for ν_c. For other directions of propagation or other modes, ν_c can be much smaller than 1° and the effect would probably be unobservable.

III. EXPERIMENTAL TECHNIQUE

The condition for the observation of the geometric resonance at the minimum frequency of 12 megacycles for all orientations and modes requires that the mean free path l exceed the maximum wavelength of the sound waves so that l should be >0.25 mm. Due to phonon scattering, this condition will be satisfied only at very low temperatures. If the impurity scattering cross section is taken to be of the order of 10^{-16} cm^2, this condition implies that the impurity concentration must be less than 10^{15} atoms/cc.

To obtain suitable samples the 99.999% pure bismuth commercially available was zone refined[24] using 12 to 15 zone passes in a graphite boat lined with candle soot. In this manner ingots $\frac{3}{4}$ in.$\times\frac{3}{4}$ in.$\times$20 in. containing single-crystal regions a few inches long were obtained. Crystals in the middle of the ingot were oriented by the Laue back-reflection x-ray diffraction technique, and sections about 1 cm long were cut with a high-speed abrasive wheel operated under water. The resultant cold-worked layers were removed with 20% nitric acid and the ends lapped flat and parallel to 10′ with a 600 mesh SiC abrasive. Etching experiments reveal that under optimum conditions a layer of polycrystalline material about 10^{-1} mm thick is produced by the lapping operation.

Zone-refining concentrates Pb, Cu, Ag, Ni, and Fe in the discarded ends of the ingot. Semiquantitative spectrographic analysis of the samples themselves reveal only Cu and Ag in concentrations less than 0.3 ppm by weight, as judged by comparison with standard samples. Gas analysis indicates that total weight concentration of volatile impurities is less than 10^{-7}.

The least pure sample (as judged from the amplitude of the observed geometric oscillatory effects) used in these experiments had a residual resistance at 1.2°K equal to 1/220 of its resistance at 300°K. Microwave measurements of surface impedance in the extreme anomalous region kindly made by Mr. George Smith on this sample, combined with dc resistivity data, yield a value for the mean free path of the electrons in a plane perpendicular to the trigonal axis of 0.14 mm. Similar data on other samples indicate that the mean free path is somewhat larger. In any case, this criterion on mean free path for the observance of geometric resonance for electrons is not met for all of the experimental situations which were tried. Furthermore, evi-

[24] W. P. Pfann, *Solid-State Physics*, edited by F. Seitz and D. Turnbull (Academic Press, Inc., New York, 1957), Vol. 4, p. 424.

dence from surface impedance experiments coupled with dc data indicate that the mean free path for holes is probably significantly less than for electrons. It is not surprising therefore that certain experiments yielded negative results. A quartz transducer of 12 Mc/sec fundamental frequency was attached to each end of the sample using a water soluble stopcock grease as adhesive. The transducers were X-cut or Y-cut so that either longitudinal or transverse waves could be generated in the sample, in pulsed or continuous operation at frequencies up to the seventh harmonic. The quartz crystals were $\frac{3}{4}$ in. in diameter with gold electrodes evaporated in such a way that the equivalent active diameter was $\frac{3}{8}$ in. The electrodes were arranged in the manner described by Huntington[25] to facilitate electrical connections on one side.

The sample was suspended directly in liquid He at the end of two monel coaxial lines in a standard cryogenic arrangement schematically shown in Fig. 2. The temperature up to the boiling point of the liquid He was controlled by pumping and measured with a vapor pressure thermometer. Data at higher temperatures were obtained by surrounding the sample with a copper can containing 80 g of charcoal and allowing the whole unit to warm up at a rate which was 0.2% per minute at 6°K. Temperatures between 20°K and room temperature were measured with a calibrated copper-constantan thermocouple. Between 4.2°K and 20°K, the temperature was interpolated with the aid of a carbon resistance thermometer. The field H_0 was generated by passing a current from an electronically regulated generator through a pair of Helmholtz coils. The field was homogeneous to 1% over the region occupied by the sample and was measured by a bismuth magnetoresistance probe calibrated by means of a proton magnetic resonance detector.

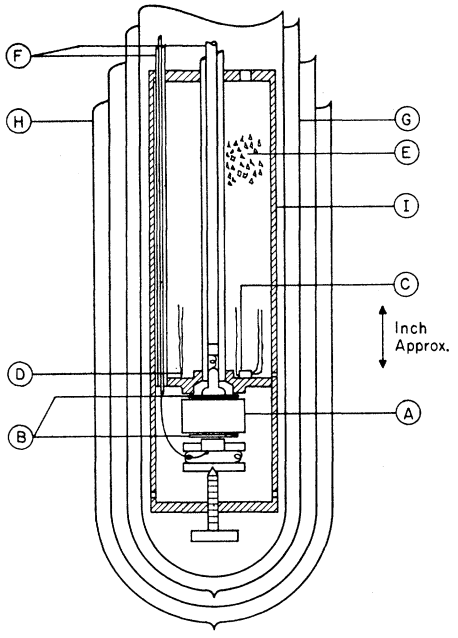

FIG. 2. Cryogenic arrangement. (*A*) Sample; (*B*) tranducers; (*C*) carbon resistance thermometer; (*D*) thermocouple; (*E*) charcoal; (*F*) coaxial lines; (*G*) Pyrex helium Dewar; (*H*) nitrogen Dewar; (*I*) copper can.

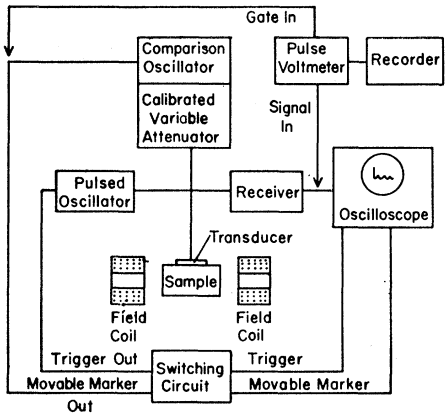

FIG. 3. Block diagram of pulse echo technique. The comparison oscillator is a Hewlett-Packard model 608C. It includes a continuously variable attenuator. The pulse voltmeter arrangement is also shown.

The technique used to measure the attenuation of pulses, shown schematically in Fig. 3, is an adaptation of that used by Truell.[26] To avoid errors arising from variations in receiver gain, a continuously variable rf comparison pulse from a stable oscillator was placed adjacent in time to any desired echo pulse and adjusted to the same height as the latter on the display oscillograph. The calibrated attenuation required to bring the pulse heights in coincidence was used as a measure of the attenuation suffered by the echo pulse. To facilitate the measurement of the attenuation as a function of magnetic field, a peak reading voltmeter capable of selecting a given echo was used to drive a recording potentiometer. The magnetic field was caused to increase approximately linearly with time so that this recording gave a direct plot of pulse height *versus* field.

We anticipate the data presented in the next section to remark that the oscillatory field dependence of the attenuation reported here usually has a maximum amplitude of a few percent of the total attenuation. For this reason, we used a continuous wave technique, similar to that used in nuclear magnetic resonance studies.[27] In this technique, illustrated schematically in Fig. 4, a small sinusoidal variation $H_1 \sin\omega t$ is superimposed on the steady magnetic field H_0, where $H_1 \ll H_0$ and could be varied from 3 to 50 oersteds. The

[25] H. B. Huntington, Phys. Rev. **72**, 321 (1957).

[26] R. L. Roderick and Rohn Truell, J. Appl. Phys. **23**, 267 (1952).

[27] E. R. Andrew, *Nuclear Magnetic Resonance* (Cambridge University Press, Cambridge, 1955), Chap. III. We are grateful to Dr. Frederick Reif for suggesting the use of this technique.

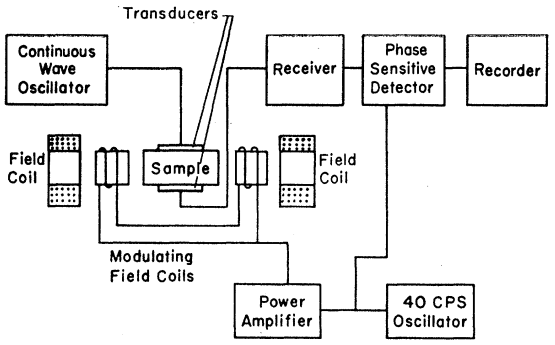

FIG. 4. Block diagram of the continuous wave method. The receiver was a standard superheterodyne type. A Hewlett-Packard 608C oscillator was used to generate the continuous wave.

signal from the detecting transducer is thus modulated at a frequency of 40 cps. This amplitude modulated radio wave is amplified with a superheterodyne receiver and the 40-cps modulation signal rectified with a phase sensitive detector. The resultant dc signal is proportional to the rate of change of transmitted amplitude A with field, that is $(1/A_0)(dA/dH)$. The negative of this quantity is automatically recorded as a function of time. During these measurements the copper can surrounding the sample was removed to minimize eddy current shielding.

The amplitude is given exactly by $A=A_0e^{-C\alpha L}$, where L is the length of the sample and C converts db/cm to the proper units. To a satisfactory approximation under our experimental conditions the exponential can be expanded so that the measured quantity is nearly proportional to $d\alpha/dH$. In the free-electron theory of Cohen, Harrison, and Harrison,[16] maxima occur in $d\alpha/dH$ for orbital diameters given approximately by

$$d=(n+\tfrac{1}{2})\lambda. \tag{15}$$

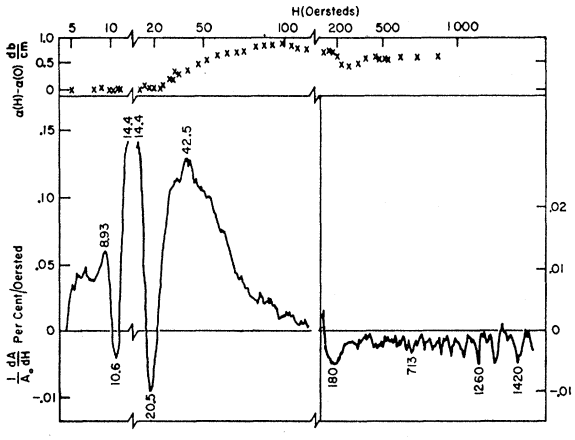

FIG. 5. Field dependent part of the attenuation and derivative of transmitted amplitude plotted *versus* field in three field ranges, $H_0\|y$. 60 Mc/sec longitudinal mode along x axis. The peaks at low fields are Type I. The peak at 180 oersteds is of Type II. The oscillations above 700 oersteds are Type III. The field scale is not quite linear. The absolute value of the derivatives is accurate to ±50%.

The period of oscillations is essentially the same for both α and $d\alpha/dH$.

IV. EXPERIMENTAL RESULTS

In the interests of clarity, we present the data in the order of emphasis. First we discuss the full magnetic field dependence of the attenuation of 60-Mc/sec longitudinal waves propagated along the x axis in the crystal for H_0 along y and z. We then discuss how the phenomena observed in these two simple cases vary as the magnetic field direction is changed, both in the y-z plane and the x-y planes. Finally, we discuss the variation of the attenuation with temperature and with frequency in certain cases and point out that the sparser data obtained for the attenuation of shear waves supports the general picture inferred from the study of longitudinal waves.

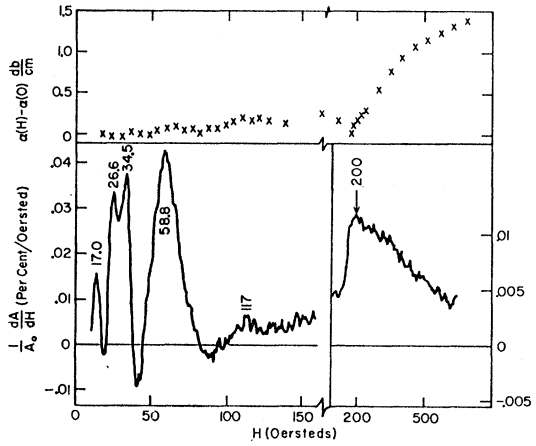

FIG. 6. Field dependent part of the attenuation and derivative of transmitted amplitude plotted *versus* field. $H\|z$, 60 Mc/sec longitudinal mode along x axis. All peaks are Type I, Type III peaks for this orientation would occur at a few kilo-oersted, beyond our range of measurement. The absolute value of the derivative is accurate to ±50%.

A panoramic view of the field dependence of α for the case of 60-Mc/sec sound waves propagated along the x axis at 1.2°K is shown in Fig. 5 for the field along the y axis and in Fig. 6 for the field along the z axis. In both figures the upper curve is the difference between α in a magnetic field and α in zero field as measured by the pulse method. The lower curve in each case shows $-dA/dH$ obtained with the continuous wave method. The principal features of these curves are (*a*) a general increasing trend of α as the magnetic field is increased which saturates at fields below 1000 oersteds, (*b*) the existence of a set of oscillations (called Type I) at fields of order 100 erosteds, (*c*) the appearance of a weaker set of oscillation (Type II) in the intermediate field range of a few hundred oersteds, and (*d*) the existence of a set of oscillations (Type III) in the saturation field range starting at 700 to 1000 oersteds.

The various sets of oscillations, all of which appear

upon analysis to be either periodic in $1/H$ or superpositions of oscillations of different period in $1/H$, depend in characteristically different ways upon the experimental parameters. As may be seen from Fig. 7 the fields at which the peaks of the low fields oscillations (Type I) occur are proportional to the frequency. However, comparison between experiments with shear waves and longitudinal waves of the same frequency indicates that the Type I oscillations actually scale with λ rather than frequency. The Type III oscillations on the other hand are independent of frequency and mode of propagation. As we shall show in detail later, the orientation dependences of the Type I and Type III oscillations are quite different. For Type I oscillations, the highest field peak in $-dA/dH$ occurs at a value of $1/H_0$ approximately equal to half the period in $1/H_0$.

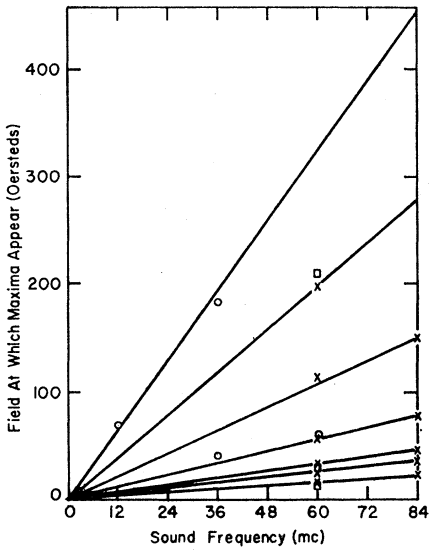

FIG. 7. Magnetic field values at which Type I peaks occur *versus* frequency. $H\|Z$; 60 Mc/sec longitudinal mode along x axis. Symbols refer to repeated measurements.

The apparent period of the Type II oscillations, however, does not satisfy this relation. This fact is the principal reason for distinguishing the Type II oscillations as a separate set. The data on the Type II oscillations is not as complete as for the Type I and Type III oscillations, but those which are available indicate that the frequency and mode dependences are qualitatively similar to those observed with the pulse echo technique which yielded only barely discernible traces of the Type I oscillations. Both sets of oscillations are seen with the continuous wave apparatus, the Type I appearing larger than the Type II partly because the sensitivity of the continuous wave technique decreases as $1/H^2$ for a constant modulating field.

It should be emphasized that the effect of the magnetic field on the attenuation is observable only at temperatures of order of 10°K. The saturation value of

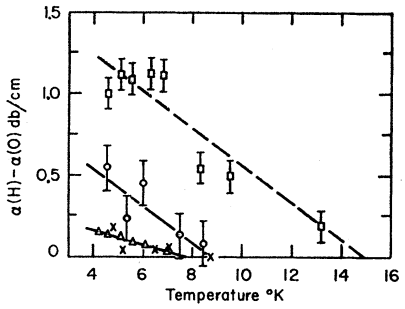

FIG. 8. Frequency and temperature dependence of the saturation value of $\alpha(H)-\alpha(0)$; □—84 Mc/sec longitudinal mode along z axis $H\|y$, 287 oe; ○—36 Mc/sec shear mode along z axis $H\|x$, 459 oe; ×—12 Mc/sec longitudinal mode along z axis $H\|x$, 459 oe; △—12 Mc/sec longitudinal mode along z axis $H\|y$, 287 oe.

α varied with temperature and frequency in the manner shown in Fig. 8. Qualitatively, the amplitude of the oscillations varies in the same manner with temperature as the saturation value.

We now turn to a description of the orientation effects. In Fig. 9, the saturation value of the attenuation of a 60-megacycle longitudinal wave propagated along the x axis is shown as a function of the angle of rotation of H_0 in the y-x plane (curve D). Curves B and C show the saturation attenuation of the two 12 Mc/sec shear modes propagating along the x axis as a function of the direction of H_0 in the y-z plane. All the curves should have 180° rotation symmetry. It is important to note how narrow the lobes associated with the polar plot in the x-y plane are compared with those of the y-z plane. The x-y plane plots for the shear modes are not shown but they consisted of a *single* lobe less than 4° wide at half height. As a consequence of this,

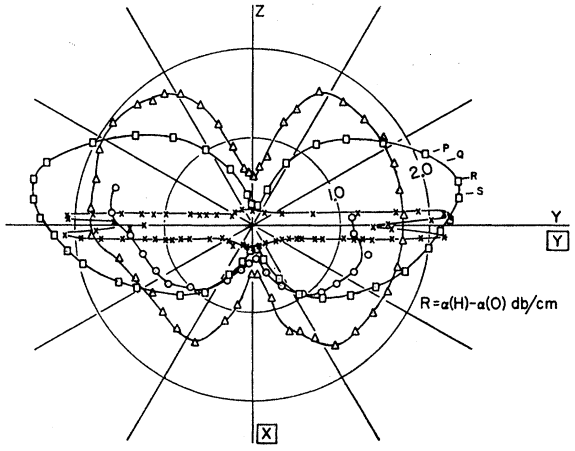

FIG. 9. $\alpha(H)-\alpha(0)$ *versus* field direction. $q\|x$. For the curves with ○, △, □ the field was rotated in a plane normal to **q**. For the curve with × points the field was rotated in the x-y plane. The boxed labels on the axes refer to this curve. (*A*) △ longitudinal mode 60 Mc/sec, 230 oe, 4.2°K; (*B*) ○ Fast shear mode 12 Mc/sec, 138 oe, 1.2°K (divide attenuation scale by three); (*C*) □ Slow shear mode 12 Mc/sec, 103 oe, 1.2°K; (*D*) × longitudinal mode 60 Mc/sec, 230 oe, 4.2°K.

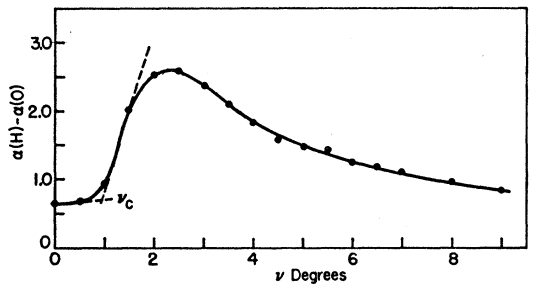

FIG. 10. One lobe of the fork effect curve for 60 Mc/sec longitudinal mode along the x axis, **H** at an angle of ν from the y axis in the x-y plane. $H=276$ oe, $T=1.2$°K, showing how ν_c was measured.

small alignment errors may result in relatively large departures from 180° rotational symmetry. The fields at which some of the polar plots in Fig. 9 were made not large enough to produce saturation when the field was near the z axis. Nevertheless, other data not shown indicate that the saturation value is indeed smaller when H is near the z axis so that Fig. 9 does represent the general anisotropy of the saturation attenuation.

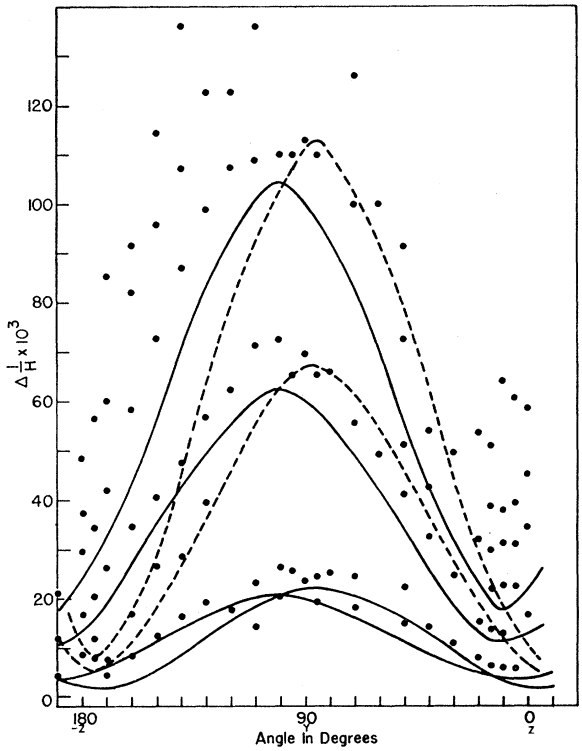

FIG. 11. The calculated curves of peak position of $-1/A_0\,dA/dH$ are calculated for $\alpha_{11}=179$, $\alpha_{22}=1$, $\alpha_{33}=84.5$, $\alpha_{23}=+7.2$ and Shoenberg's value of $E_c=2.83\times10^{-14}$ erg (0.017_7 ev). The first peak position is plotted at a value of $1/H$ equal to half the period in $1/H$. This choice gives good agreement with the data for the fields near the y axis but for the fields near the z axis the agreement is not so good as it would be if the first peak were plotted at about (6/7) of the period. The periods calculated at both directions are in reasonable agreement with the data, since in fact the α_{ij} used were derived from these periods.

A second important feature of the orientation dependence is the sharp minimum in the attenuation curve D of Fig. 9 which occurs when H_0 is perpendicular to the direction of propagation of the longitudinal wave. The lobes are sharper at lower temperatures (see Fig. 10) or higher frequencies, but the separation angle is independent of frequency and temperature. An explanation of this phenomenon, which we call the fork effect, is implied in the previous section and made explicit in the next section.

The most significant data are obtained by measuring the attenuation as a function of field for various angles in a plane perpendicular to the propagation direction such as at points P, Q, R, S, etc., on Fig. 9. This has been done for the conditions noted in Table I. The periods $\Delta(1/H_0)$ of both Type I and Type III oscillations may then be determined as a function of field direction. A plot of peak positions *versus* angle for the

TABLE I. Observation of Type I effects.[a]

Propagation axis	Mode	Field direction	Frequency (Mc/sec)	Temperature °K
x	longitudinal	y-z plane	12, 36, 60, 84	4.2, 1.2
z	shear	x-y plane	12	1.2
x	slow shear	y-z plane	12	1.2

[a] A different sample was used for each of the three experiments. The data from the longitudinal mode, which are analyzed in detail, are superior to those from the shear modes.

TABLE II. Observation of Type III oscillations.

Propagation axis	Mode	Field direction
x	slow shear	near y-axis and 45° in y-z plane
x	slow shear	various directions in x-y plane
x	longitudinal	x-y plane
z	shear	x-y plane
x	longitudinal	within about 45° of y-axis, y-z plane
x	slow shear	y-axis

Type I oscillations is shown in Fig. 11. Figure 12 shows more extensive data on the Type III oscillations. A plot of the period *versus* angle for the Type III oscillations is shown in Fig. 13. This figure shows clearly that the period of the Type III oscillations determined from the experiments with shear waves is the same as that determined using longitudinal waves which is not the case for the Type I oscillations. Other observations of Type III oscillations are listed in Table II. In the course of these experiments, Type II oscillations were observed under a variety of circumstances noted in Table III. Two of the best examples of Type II behavior are shown in Fig. 14.

At all temperatures studied the magnitude of the attenuation depended approximately linearly on frequency. This data is summarized in Table IV. The uncertainties in these results are large, being 10% at any given temperature for a given run with a scatter

as big as 20% between various runs. The attenuation measured on two different samples under nominally the same conditions reproduced to a factor of two or better.

Typical examples of the observed temperature dependence of α are shown in Fig. 15. The situation appears to be complicated and much more experimentation is needed before a clear picture can be drawn.

To interpret the results it was necessary to know the velocity of sound in bismuth for the various modes and directions investigated. These values are given in Table V. For completeness, the measurements were

TABLE III. Observation of Type II oscillations.

Temperature °K	Frequency Mc/sec	Mode	Prop. direct. θ	Prop. direct. φ	Field direct. θ	Field direct. φ	$1/H_0$ oersted^{-1}
1.3	12	fast shear		x		y	0.036
4.2, 1.2	12	slow shear		x		y	0.0032
1.5	12	longitudinal		x		y	0.0023
4.2	60	longitudinal		x	90°	92.7°	0.0018
1.2	60	longitudinal		x	90°	92.7°	0.0024
1.2	12	longitudinal	39°	199°	56°	55°	0.0165
	60	longitudinal	39°	199°	56°	55°	0.0027

TABLE IV. Zero-field attenuation. The shear mode attenuation at 300°K was not measured since the attenuation in the transducer bond was large at this temperature. At some temperatures the attenuation at the higher frequencies was too large to measure so only the attenuation at 12 Mc/sec is reported.

Propagation direction	Mode	Temperature °K	Attenuation ±20% $\alpha(f)$ db/cm (f in Mc/sec)
x axis	longitudinal	300	$\alpha(f)=0.5+0.07f$
		78	$\alpha(f)=0.1+0.087f$
		4.2	$\alpha(f)=0.5+0.12f$
x axis	fast shear	78	$\alpha(f)=0.0+0.34f$
		4.2	$\alpha(12)=2.0$
x axis	slow shear	78	$\alpha(f)=6.2+0.4f$
		4.2	$\alpha(12)=5.6$
z axis	longitudinal	300	$\alpha(f)=-1.5+0.16f$
		83	$\alpha(f)=0.0+0.092f$
		4.2	$\alpha(f)=0.1+0.073f$
z axis	shear	78	$\alpha(f)=3.0+0.31f$
		4.2	$\alpha(12)=8.02$
$\theta=90$, $\varphi=199$	longitudinal	300	$\alpha(f)=0.0+0.034f$
		78	$\alpha(f)=0.184+0.058f$
		4.2	$\alpha(12)=0.665$

extended so that all six elastic constants could be determined at 4.2°K, 78°K, and 300°K. In the interest of brevity, the resulting data will be reported elsewhere.

V. DISCUSSION

In this section we first demonstrate that the theoretical discussion of Sec. II can account for most of our observations if we use previously determined values of the band structure parameters. Having established the validity of the theoretical picture, we then assess the efficacy of ultrasonic attenuation as a tool for the independent determination of these parameters by calculating them directly from our observations.

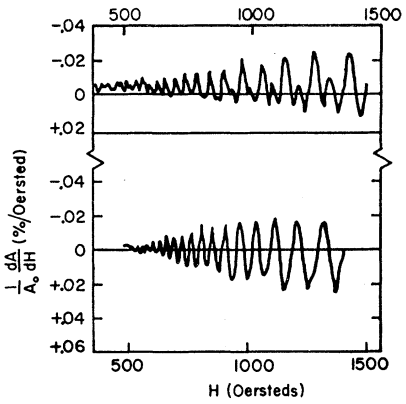

FIG. 12. de Haas-van Alphen oscillations; shear mode along z axis. Upper curve for $H \| y$ showing two periods superimposed. Lower curve for H in x-y plane, $\varphi=60°$.

We turn first to the Type I oscillations. Because the periods of these oscillations scale with λ and the first peak of $-dA/dH$ *vs* $1/H_0$ occurs at half the period, we identify the Type I oscillations as geometric resonances on the basis of Eq. (15). The magnitudes and anisotropies of the periods are very close to those computed for electrons from Eqs. (6)–(8) (using parameters derived from the present experiments, which do not differ significantly from Aubrey's mass parameters,[19] and Shoenberg's Fermi energy) as shown in Fig. 10 and discussed below.

Because the periods of Type III oscillations are independent of the frequency and mode of the sound wave, we identify them as de Haas-van Alphen oscillations. The magnitudes and anisotropies of the periods indicate that these too are associated with electrons. The three curves drawn in Fig. 12 are the periods calculated as a function of field direction in the x-y plane for each of the three sets of ellipsoids. The calculations

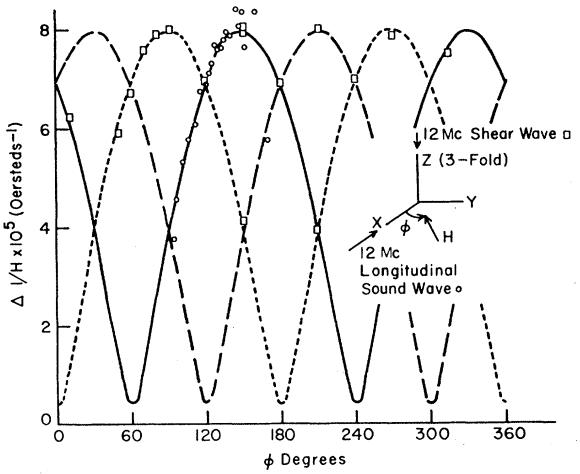

FIG. 13. de Haas-van Alphen periods *versus* field direction. The dotted curve is calculated from electron ellipsoid 1 using mass parameters adjusted to give the best fit. Dashed and solid curves are from rotated ellipsoids.

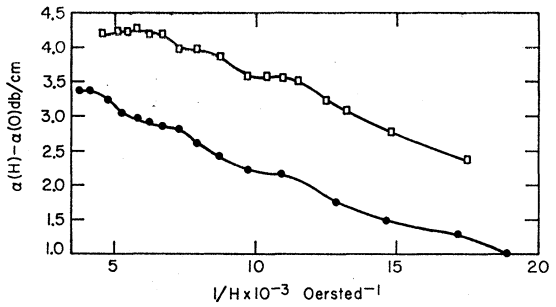

FIG. 14. $\alpha(H)-\alpha(0)$ *versus* reciprocal field. □ 1.2°K, ● 4.2°K, 12 Mc/sec, $H\|y$, slow shear along x axis. Typical Type II oscillations occur at both temperatures.

were made by assuming a value for the maximum period 5% smaller than that reported by Shoenberg and by deriving the minimum period, which can only be observed outside our field range, from an average of published parameters. The fit to our data is excellent and not sensitive to the value of the minimum period assumed.

All experiments for which $\mathbf{H}_0\cdot\mathbf{q}=0$ exhibited the saturation effect, $\alpha(H)-\alpha(0)$ at saturation being an order of magnitude larger than the amplitude of the geometric resonance oscillations. In contrast to the observed behavior in copper,[4] as previously noted,[28] the attenuation of sound in bismuth is larger in the saturation region than in zero field. The saturation behavior of the longitudinal waves is consistent with the theory of Cohen, Harrison, and Harrison[16] for large ql. The increase in α upon saturation observed for shear modes, however, does not occur in their free-electron theory. The saturation value of α measured at $H_0=1200$ oersteds is less in those directions for which the component of $\mathbf{p}\perp\mathbf{H}_0$ is large, i.e., when the condition $d<\lambda$ may not be so well satisfied.

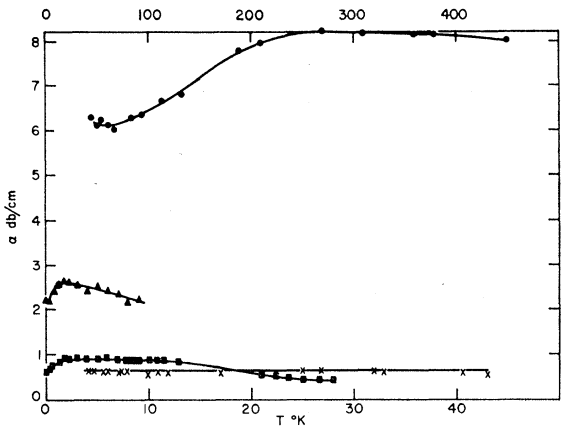

FIG. 15. Zero-field attenuation *versus* temperature × 12 Mc/sec, ● 84 Mc/sec, longitudinal mode along x axis; use lower temperature scale. ■ 12 Mc/sec, ▲ 36 Mc/sec, pseudo-longitudinal mode along $\varphi=199$, $\theta=39$; use upper temperature scale.

[28] M. J. Harrison, Phys. Rev. Letters **1**, 442 (1958).

The fork effect described in Sec. II is strikingly displayed by the attenuation of longitudinal waves with $\mathbf{q}\|x$ and $\mathbf{H}_0$ at an angle ν from the y axis in the x-y plane. See Fig. 9, *D*. These are the optimal conditions for observation of the effect because v_s is a maximum and $(\bar{v}_H)_{\max}$ is near its minimum. The critical angle ν_c for the onset of "surf riding" derived from the data in Fig. 9, *D* is 0.9_5^0, in excellent agreement with that calculated for electrons from Eqs. (12)–(14) with the known parameters for Bi. The observed independence of ν_c on frequency and temperature is consistent with this explanation. Corresponding calculations for situations in which no fork effect was observed indicated that ν_c was very much smaller. The unique feature of the fork effect is that it permits a direct determination of the Fermi velocity. In particular, for ellipsoidal Fermi surfaces, a more elaborate study of the fork effect might provide a new technique for determination of the Fermi energy, E_f. The oscillatory effects all depend on the reciprocal mass parameters α_{ij} and E_f through the combination α_{ij}/E_f. The critical angle ν_c, however, depends on the combination $\alpha_{ij}E_f$.

TABLE V. Sound velocity for orientations of interest at 4.2°K.[a]

Propagation axis	Mode	Velocity cm/sec
x	longitudinal	2.62×10^5
	slow shear	0.892×10^5
	fast shear	1.64×10^5
z	longitudinal	2.02×10^5
	shear	1.13×10^5
$\theta=39°$, $\varphi=199°$	pseudo-longitudinal	2.62×10^5

[a] A complete determination of the six elastic constants will be published shortly.

It is thus possible to determine the values of α_{ij} and E_f by ultrasonic experiments alone. The present experiments determine E_e only to an accuracy of 30%, $E_e=3.5\times10^{-14}$ erg, but more refined experiments should reduce this error materially.

For the various modes and frequencies investigated, the attenuation decreased very sharply as the component of $\mathbf{H}_0$ along $\mathbf{q}$ increased. This feature of the attenuation occurs also in the free-electron theory.[14,15]

The Type II oscillations occur in a region of H_0 appropriate for geometric resonance of holes. Furthermore, the general dependence of the oscillations on wavelength and mode of propagation is consistent with a geometric resonance. However, the observed periods $\Delta(1/H_0)$ are longer than theoretically predicted. Currently, no adequate explanation of these oscillations is available.

Having established the nature of the Type I and Type III oscillations, we may now use them to determine ratios of the reciprocal mass parameters. The period of the geometric resonance for $\mathbf{H}_0$ along y is determined by α_{33}/E_e. The maximum period of the

Type III oscillations is determined by the combination $\alpha_{11}\alpha_{33}/E_e^2$. For each order of geometric resonance, one curve of peak position *versus* orientation in Fig. 10 pertains to ellipsoids 1 and the other to ellipsoids 2 and 3. The angular displacement of corresponding extrema of the two curves is approximately proportional to $\alpha_{23}/(\alpha_{22}-\alpha_{33})$. The minimum period of the geometric resonances of ellipsoids 2 and 3 is determined approximately by the combinations $(\alpha_{11}+3\alpha_{22})/\alpha_{22}$. The foregoing four quantities therefore suffice to determine the ratios of the α_{ij} and with $E_e=0.017_7$ ev, lead to the values of α_{ij} given in Table VI.

It should be noted that we have reported a *positive* value of α_{23} in Table VI, whereas other workers report a negative value. Smith[20] has pointed out that the relation between m_{23}^* and α_{23} given by Shoenberg[8] contains an error of sign (m_4^* and α_4 in Shoenberg's notation). Shoenberg reports a negative value of m_{23}^* which, with the proper sign in his equation, would lead to a positive value of α_{23}. We suspect that this error in sign has propagated through the literature. The agreement of our results with the theory and of the magnitudes of our α_{ij} with previously reported magnitudes is improved by choosing α_{23} positive.

TABLE VI. Comparison of published mass parameters for electrons and holes in bismuth. Shoenberg's value of $E_e=0.017_7$ ev was used with all the parameters below except those of Brailsford and Galt. The independent value of E_e was calculated using the ratios of the α_{ij} from sound attenuation and the critical angle of the fork effect.

	Shoenberg[a] de Haas-van Alphen susceptibility	Aubrey and Chambers[b] Cyclotron resonance	Brailsford and Galt[c] Cyclotron resonance	Later Aubrey[d] Cyclotron resonance	Reneker Sound attenuation
α_{11}	420	168	114	202	179±10%
α_{22}	0.8	2	1.38	1.67	1.1±10%
α_{33}	40	100	106.8	83.8	84.5±10%
α_{23}	−4	−10	−9.38	−8.33	+7.2±15%
E_e	0.017_7 ev				0.022±30% ev

	Aubrey and Chambers[b]	Brailsford and Galt[c]	Smith[e]
β_{11}	0.71	14.7	1.78
β_{33}	0.19	1.09	0.114
E_h	0.7×10^{-3}		0.9×10^{-3} ev

[a] See reference 8.
[b] See reference 10.
[c] See reference 11.
[d] J. E. Aubrey (private communication).
[e] G. E. Smith (to be published). We are grateful to Mr. Smith for allowing us to use the results of his measurements for these calculations before publication.

ACKNOWLEDGMENTS

The author wishes to express his gratitude to his sponsor, Professor A. W. Lawson, for continued support and encouragement. A number of the experiments reported above resulted from frequent stimulating conversations with M. J. Harrison. Professor M. H. Cohen and M. J. Harrison were responsible in large measure for the simple theoretical model used here, which is based on a more detailed theory developed by them in collaboration with Dr. W. A. Harrison. The author is also indebted to Professor A. B. Pippard, Professor R. W. Morse, and Dr. H. E. Bömmel for enlightening discussions. The experimental work was supported by grants from the National Science Foundation, and by the Industrial Sponsors of the Institute for the Study of Metals.